

Temporal Superresolution Mapping of Ultrafast Coherent Dynamics in Terahertz-assisted Laser Field

Yizhu Zhang,¹ Tian-Min Yan,^{1,*} and Y. H. Jiang^{1,2,3,†}

¹Shanghai Advanced Research Institute, Chinese Academy of Sciences, Shanghai 201210, China

²University of Chinese Academy of Sciences, Beijing 100049, China

³ShanghaiTech University, Shanghai 201210, China

Quantum coherence is of potential applications from quantum computation using simple atoms to optimized energy transports in biomolecular complexes. Here, a time-resolved spectroscopic protocol exploiting a terahertz-assisted field locked with the probe pulse is proposed for full observations of the evolution of elements in transient density matrix. Coherence contributions of off-diagonal elements are detectable in the spotlight. The coherence dynamics for photoexcitation of hydrogen atom are explicitly demonstrated with significantly improved temporal resolution beyond the probe pulse duration. Present approach with improving time resolution and highlighting coherence dynamics displays potential applications for sub-femtosecond or attosecond time-resolved measurements in free electron lasers and tabletop laser fields.

Quantum coherence derived from the principle of superposition is a fundamental concept in quantum mechanics and a ubiquitous phenomenon with the time scale ranging from milliseconds, as in delicately prepared cold atoms, to attoseconds for electronic coherence in field-perturbed atoms [1] and molecules [2]. Although the coherence dynamics take a key role in photo-reactions [3–5], the real-time observation of electronic coherence is highly challenging, particularly on the femtosecond or even attosecond time scale. In photo-ionization processes in atoms and molecules, the electronic coherence prepared by shaking the inner-shell electrons has been predicted to lose within one femtosecond. The decoherence is closely related to the correlation between the photoelectron and the parent ion, significantly affecting the formation of coherent hole wave packets in atoms or molecules [1, 2]. In addition, for the recently investigated photosynthetic complexes, the possible mechanism of coherence-assisted energy transfer is explored by the multi-dimensional optical spectroscopy, while it still requires further supporting evidences from experimental observations when multiple transport pathways are involved in the extremely complicated biomolecular environment. The observation of ultrafast electronic coherence dynamics is indispensable to provide valuable insight into these fundamental processes. Despite of the significance, ultrafast coherence dynamics are not readily obtained from commonly used time-resolved (pump-probe) spectroscopies, since the comparatively large population signal usually conceals the signature of the coherence.

The complete dynamic information of an open quantum system is encoded in the time-evolved density matrix $\rho(\tau)$, where the population and the coherence are represented by diagonal and off-diagonal elements, respectively. The reconstruction of $\rho(\tau)$ from dedicated designed experiments, e.g., the multi-dimensional spectroscopy, is always useful. The full description of a quantum black-box is achievable by realizing the quantum process tomography with the multi-dimensional spec-

troscopy [6]. The temporal resolution of optical spectroscopy, however, is restricted to the timescale of tens of femtoseconds. Since the quantum states are typically prepared and probed by femtosecond-duration pulses, the convolution with the probing pulse leads to the smear of signatures of faster electronic coherences.

In this sense, observing the ultrafast electronic coherence in atoms and molecules, in principle, requires the attosecond metrology. Exploiting the attosecond transient absorption spectroscopy, the electronic coherence of the valence electron in krypton ions was measured with the sub-femtosecond temporal accuracy [7]. The same spectroscopic methodology also allows observing the correlated two-electron coherence motion in helium with attosecond temporal resolution [8]. Although the attosecond metrology can probe the electron wavepacket motion with high temporal resolution, it requires tremendous efforts with sophisticated laser techniques, including the precise control of both the amplitude and phase of the femtosecond light field throughout the measurement. Moreover, contributions from population and coherence are overlapped after one-dimensional spectral projections, thus usually concealing quantum coherence. For the recently developed free-electron-laser (FEL) facilities, the compression of the pulse with high energetic photons (from extreme ultraviolet to hard X-ray region) down to the sub-femtosecond scale is difficult, obstructing further insights into ultrafast electronic coherence. Kowalewski *et al.* proposed to record the sub-femtosecond electronic coherence using a femtosecond probe pulse [9]. The photoelectron is driven by a phase-locked near infrared (NIR) pulse and multiple sidebands around the characteristic peaks are created. The sidebands carry the high-resolution information of coherence, yet simultaneously complicate the spectroscopic analysis due to the possibly contaminated characteristic spectral features. Moreover, the prerequisite that the photon energy of the streaking field has to be resonant with the relevant states may become a restriction.

In this work, we propose a spectroscopic method to retrieve the full information of the density matrix, like the two-dimensional spectroscopy, unravelling the contributions of coherence in an extra dimension. Moreover, the temporal resolution of the method is much less restricted by the duration of the probing field than in the conventional spectroscopy. The sub-femtosecond resolution is accessible, approaching the impulsive response limit. Exploiting the femtosecond extreme ultraviolet (XUV) pulse and terahertz (THz) streaking field, we show density matrix elements can be directly mapped into the photoelectron spectra. Conventionally, the streaking technique is used to characterize the temporal profile of ultrashort pulses, e.g., the attosecond streaking technique that calibrates an attosecond pulse using a moderately strong NIR light field [10], the FEL calibration using the THz or IR-streaking pulse [11–13]. Here, instead of field diagnosis, the THz-streaking technique is used to investigate ultrafast dynamics. In contrast to proposals operating in the so called "sideband regime" [9], our method works in the "streaking regime" [13]. The method is particularly designed for FEL time-resolved experiments, significantly increasing the temporal resolution. The attosecond resolution, as claimed by attosecond transient spectroscopies, is attainable, overcoming the limitation of resolution that is set by the large duration of an FEL pulse [14]. Nowadays, only the motion of molecular vibrational wave packet can be observed with FEL pump-probe measurements. Our method in principle allows observing the motion of the electronic wave packet in FEL facilities, and also helps improve the temporal resolution of tabletop ultrafast experiments. Moreover, without the restriction that the photon energy must match the energy gap between coherently excited states, the method allows for the direct applications in systems without *a priori* knowledge.

The scheme of the streaking-assisted photo-ionization is illustrated in Fig. 1(a). Assuming that a two-level system is subject to a pump pulse, the superposition of states $|g\rangle$ and $|e\rangle$, as desired to be measured, is prepared. The subsequent probe fields, as proposed in this work, comprises a femtosecond XUV pulse and a well synchronized THz pulse. The center of the XUV pulse is required to be temporally locked at the zero-crossing of the vector potential of the THz field. The combination of the two pulses allows for the most effective broadening of characteristic peaks in the photoelectron spectra or momentum distribution thanks to the effectively two-step procedure. The single-photon ionization induced by the XUV pulse liberates the electron of the superposed state. The overlapping THz wave then drives the photoelectron, kinetically separating electronic trajectories encoded by different initial information. As shown in Fig. 1, the initial information, as described by the instantaneous density matrix [Fig. 1(b)] when the electron is released, are mapped directly onto different regions in

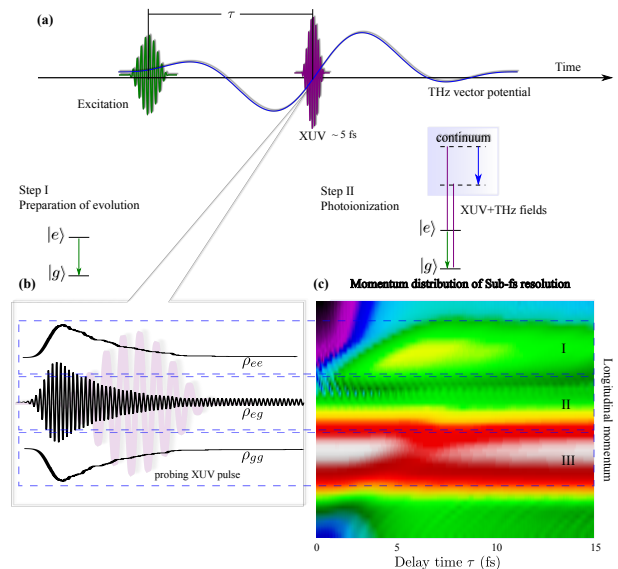


Figure 1. Schematic of the streaking-assisted photo-ionization experiment. (a) The pulse sequence configuration in the measurement. The pump pulse (green) couples a two-level system and creates the superposition state. A femtosecond XUV pulse (purple) with a well-synchronized THz streaking pulse (blue) as a probe beam scans over time delay τ . The XUV pulse is locked at the zero-crossing of the THz vector potential. The THz wave couples the two ionization pathways and exhibits the relative quantum phase between the two ionization pathways. (b) The time evolution of the density matrix. The purple shadowed line sketches the probing XUV pulse, whose duration is much longer than the oscillatory period of the quantum beat of the superposition state. (c) The well-resolved coherence dynamics in the THz-assisted photoelectron momentum spectrum. Elements of the density matrix, ρ_{gg} , ρ_{ge} and ρ_{ee} , are mapped into regions I, II and III, respectively. The two main peaks in regions I and III implicate the time evolution of populations of the ground state and excited state. The interference fringe in region II accounts for the coherence of the two-level system.

photoelectron spectrum [Fig. 1(c)]. In Fig. 1(c), regions I and III depict the time-evolved populations, which can also be measured using other time-resolved spectroscopy. The spectral features in region II are of essential concern. Scanning over the delay time τ , the fringe in region II is oscillating with the period corresponding to the energetic gap between states $|g\rangle$ and $|e\rangle$, revealing the quantum phase of the electronic wave packet. The fringes are formed by quantum interference of the photoelectron via different ionization pathways. The wave packet of free electron released from an initially superposed state is driven by the THz wave into the indistinguishable final state of the same asymptotic momentum. Therefore, the broadened spectral lines of different states overlap leading to the coherence-encoded interference pattern.

The application to excitation process of a two-level system, as demonstrated above, is straightforwardly extensible to explore multi-level or multi-excitation systems.

Besides the isolated system, the possibility to explore an open quantum system is where the method shines. The method provides an alternative tool to investigate the decoherence of attosecond photo-ionization in atoms and molecules, and the coherence energy transport in complex photo-reaction systems. In the following, the more detailed description of the principle and implementation of the method are presented.

The proposed experiment can be demonstrated by exploring the momentum distribution of photoelectron under the strong field approximation (SFA). Assuming the atom is subject to linearly polarized fields, $E(t) = E_{\text{XUV}}(t) + E_{\text{THz}}(t)$, the ionization signal of the longitudinal momentum p , $w(p) = |p||M_p|^2$, is collected along the polarization direction. Neglecting the high-order above threshold ionization, the amplitude of the direct ionization in the length gauge reads,

$$M_p(t) = \int_0^t dt' e^{iS_p(t')} \langle p + A(t') | \hat{\mu} E(t') | \Psi_0(t') \rangle, \quad (1)$$

where $A(t) = A_{\text{XUV}}(t) + A_{\text{THz}}(t)$ is the vector potential and $S_p(t') = \frac{1}{2} \int_0^{t'} dt'' [p + A(t'')]^2$. $\hat{\mu}$ is the transition dipole, and $|\Psi_0(t)\rangle$ is the initial (superposed) state. The photoelectron emission process consists of two steps. The light field firstly liberates the electron from the atom when the XUV pulse plays a dominant role. Subsequently, the photoelectron is drifted to the final momentum. Since $A_{\text{XUV}} \ll A_{\text{THz}}$, the free electron is driven almost only by the THz electric field. According to the analysis of the ionization probability in the streaking regime (see Supplementary), the population reads in the momentum distribution

$$w_{ii}(\tau) \sim \rho_{ii}(\tau) e^{-\Omega_{ii}^2(p)/2s^2(p)}, \quad (2)$$

and the coherence reads

$$w_{ij}(\tau) \sim \rho_{ij}(\tau) e^{-i\Delta_{ij}\tau} e^{-\Omega_{ij}^2(p)/2s^2(p)}, \quad (3)$$

where τ is the temporal center of the probing fields. The Gaussian profile in Eq. (2) and (3) depicts all peaks when $\Omega_{ij}(p) = 0$ is satisfied. In Eq. (2), peaks at $p_{ij}^2/2 = \omega_{\text{XUV}} - I_p^{(i)}$ represent the population of state i , where ω_{XUV} is the photon energy of XUV field and $I_p^{(i)} = -E_i$ is the ionization potential. In Eq. (3), the information of coherence ρ_{ij} is encoded at the peak p_{ij} satisfying $p_{ij}^2/2 = \omega_{\text{XUV}} - (I_p^{(i)} + I_p^{(j)})/2$. The peak for ρ_{ij} appears exactly between peaks for ρ_{ii} and ρ_{jj} . The widths of peaks are determined by $s(p) = \sqrt{1/\sigma^2 + (\alpha p \sigma)^2}$ depending on the THz field amplitude α and the XUV field duration σ . In Eq. (3), the phase factor $-i\Delta_{ij}\tau$ shows that the spectral yield is modulated along the time delay τ with period $\Delta_{ij} = I_p^{(i)} - I_p^{(j)}$. From Eq. (3), though the signal of the coherence is much smaller than the population, the visibility of the interference enhances when

the THz field increases under the linear approximation. For the energetic spaces spanning over a few eV in typical molecular transitions, the THz electric field of \sim kV/cm is sufficient to couple the coherently excited states, which is conveniently provided by tabletop THz sources nowadays.

Taking the simplest example of a two-level system, we show the feasibility to image the population and coherence using the THz-streaking method. Assuming the system is prepared in the superposed state with the equal probabilities,

$$|\Psi_0(t)\rangle = \frac{1}{\sqrt{2}}|g\rangle e^{-iE_g t} + \frac{1}{\sqrt{2}}|e\rangle e^{-iE_e t} \quad (4)$$

with $|g\rangle$ and $|e\rangle$ the ground state and excitation state of energies E_g and E_e , respectively. Here we consider a hydrogen atom with $E_g = -13.6$ eV and $E_e = -3.4$ eV. The photon energy of the XUV pulse is 54.4 eV and the duration is 5 fs. The center frequency of the single-cycle THz pulse is 4 THz and the field strength is 1 MV/cm. In principle, the requirement that XUV pulse is temporally locked at the zero-crossing of $A_{\text{THz}}(t)$ can be satisfied in the FEL facility, where the XUV and THz pulses, generated by the same electron bunch from the linear accelerator, are well synchronized [11]. Although Fourier transformation limited pulse is not conveniently delivered in the self-amplified spontaneous emission (SASE) mode, the seeding operation improves the temporal coherence and the profile of FEL pulse [15].

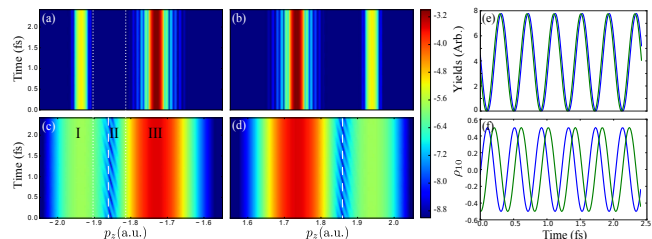


Figure 2. The super-temporally resolved quantum coherence with streaking-assisted photo-ionization. Panels (a) and (b) show the τ -dependent photoelectron momentum distribution in backward and forward directions without THz-streaking. In comparison, the results with THz-streaking are shown in panels (c) and (d). Spectral lines located at 1.73 and 1.94 a.u. are associated with photoelectrons from states $|g\rangle$ and $|e\rangle$, respectively. Panel (e) shows the temporal profile of the momentum distribution, extracted along dashed lines in panels (c) and (d) for the given momentum, in the forward (blue) and backward (green) directions. The beating pattern well recovers the coherence ρ_{eg} as shown in panel (f).

In order to resolve the quantum coherence, the probing fields scan along the time delay τ -axis, yielding the momentum distributions versus τ as shown in Fig. 2. Without the streaking THz field, panels (a) and (b) show the spectrograms for backward ($p < 0$) and forward ($p > 0$)

detections, respectively. As the kinetic energy of the photoelectron from the i th state is $\omega_{XUV} - I_p^{(i)}$, the spectral peaks at 1.73 a.u. (region I) and 1.94 a.u. (region III) originate from states $|g\rangle$ and $|e\rangle$, respectively. The spectral features in region I and III recover the population terms in Eq. (2) which are independent of τ since in Eq. (4) the amplitudes of $|g\rangle$ and $|e\rangle$ are constants. The momentum distributions with the streaking THz field are shown in Fig. 2(c) and 2(d). The spectral lines in region I and III are significantly broadened by the streaking field, and in the intermediate overlapping region (region II) fringes are formed. Extracting the data along the dashed lines in Fig. 2(c) and 2(d), in Fig. 2(e), the fringes oscillate with the period 16.75 a.u. (0.4 fs), corresponding to 10.2 eV between states $|g\rangle$ and $|e\rangle$, in good agreement to the oscillatory pattern of coherence $\rho_{eg}(\tau)$ [Fig. 3(f)]. The results verify that the fringes are associated to the quantum coherence between states $|g\rangle$ and $|e\rangle$, recovering the relative phase of electronic states. Remarkably, the THz-streaking assisted method allows for resolving the sub-femtosecond quantum beating that cannot be achieved by a 5-fs probing XUV pulse alone.

The simple two-level system has demonstrated that the density matrix can be retrieved by streaking-assisted photoelectron spectroscopy. However, the method is particularly useful when the ultrafast relaxation and decoherence dynamics in open quantum systems are of concern. Here, we show that the ultrafast decoherence can be tracked by the petahertz sampling. We consider an ensemble consisting of two-level atoms that interacts with a resonant pulse. The open quantum system is simulated using the method of Monte Carlo wave function [16], allowing for the description of spontaneous emission and decoherence (see Supplementary for details). The energies of the two-level system are $I_p^{(g)} = 13.6$ eV and $I_p^{(e)} = 3.4$ eV, and the excitation pulse has the Gaussian envelope with the duration of ~ 5 fs. The waveform-controlled pulse excites the atoms, simultaneously creating quantum coherences between states $|g\rangle$ and $|e\rangle$. After the excitation, the system undergoes the free evolution with the coherence surviving ~ 10 fs. Fig. 3(a) shows the time evolution of population (ρ_{gg} and ρ_{ee}) and coherence (ρ_{eg}).

Using the same probing fields as for the former closed system, the momentum distributions versus τ are shown in Fig. 3(c) and 3(d), respectively, in the forward and backward directions. Also, three distinct regions are present corresponding to all matrix elements of $\rho(\tau)$. The main peak in regions I (III) depicts the evolution of population in the ground (excited) state, and region II reveals the coherence of the ensemble quantum system. Reading the time evolution of momentum distribution, as indicated along the solid lines in Fig. 3(d), we find in Fig. 3(b) that both the relaxation and decoherence can be inferred from the momentum spectra versus τ . The coher-

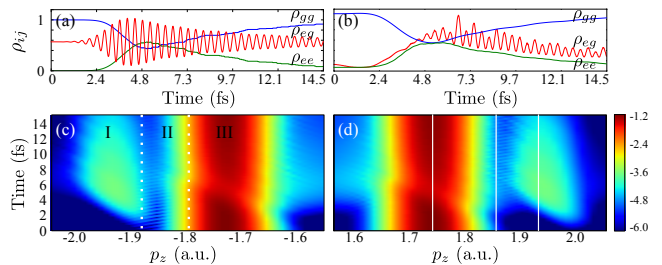


Figure 3. Mapping decoherence with the THz-assisted photoionization spectroscopy with petahertz sampling. Within the open quantum system, the time evolutions of populations, ρ_{gg} (blue), ρ_{ee} (green), and coherence, ρ_{ge} (red), are shown in panel (a). Same as in Fig. 2, panels (c) and (d) show the momentum distributions versus time delay in backward and forward directions. In panel (b), three curves represent the data extracted along the solid lines in panel (d).

ence of the system persists ~ 10 fs, and the decoherence results from the inhomogeneous behaviors of individual atoms in ensemble system. The measurement well recovers the calculated results shown in Fig. 3(a), validating the feasibility of the streaking-assisted photo-ionization spectroscopy method. The simple model demonstrates that the streaking-assisted photo-ionization spectroscopy can retrieve the complete information of density matrix containing both population elements ρ_{ii} and coherence elements ρ_{ij} on attosecond temporal accuracy. The extension of the method to explore more complex systems is straightforward with the spectroscopic protocol.

In summary, a spectroscopic protocol is proposed to fully describe the evolution of density matrix with the sub-femtosecond temporal accuracy. The time-dependent density matrix can be reconstructed from streaking-assisted photoelectron spectrum. With the XUV pulse of fs-scale width, the quantum coherence of sub-fs precision can be retrieved, less restricted by the duration of probing field than in conventional transient spectroscopies. The method offers the possibility to observe the sub-femtosecond decoherence of attosecond photo-ionization in small atomic and molecular systems. For more complex systems, e.g., biological molecules and complexes, the coherent energy transfer in photosynthetic complexes may also be investigated with unprecedented temporal resolution.

The study was supported by National Natural Science Foundation of China (NSFC) (11420101003, 61675213, 11604347, 91636105), National Basic Research Program of China (2013CB922200), Shanghai Sailing Program (16YF1412600).

* yantm@sari.ac.cn
† jiangyh@sari.ac.cn

- [1] S. Pabst, L. Greenman, P. J. Ho, D. A. Mazziotti, and R. Santra, *Phys. Rev. Lett.* **106**, 053003 (2011).
- [2] C. Arnold, O. Vendrell, and R. Santra, *Phys. Rev. A* **95**, 033425 (2017).
- [3] G. S. Engel, T. R. Calhoun, E. L. Read, T.-K. Ahn, T. Mančal, Y.-C. Cheng, R. E. Blankenship, and G. R. Fleming, *Nature* **446**, 782 (2007).
- [4] E. Collini and G. D. Scholes, *Science* **323**, 369 (2009).
- [5] E. Collini, C. Y. Wong, K. E. Wilk, P. M. G. Curmi, P. Brumer, and G. D. Scholes, *Nature* **463**, 644 (2010).
- [6] J. Yuen-Zhou, J. J. Krich, M. Mohseni, and A. Aspuru-Guzik, *Proc. Nat. Acad. Sci.* **108**, 17615 (2011).
- [7] E. Goulielmakis, Z.-H. Loh, A. Wirth, R. Santra, N. Rohringer, V. S. Yakovlev, S. Zherebtsov, T. Pfeifer, A. M. Azzeer, M. F. Kling, S. R. Leone, and F. Krausz, *Nature* **466**, 739 (2010).
- [8] C. Ott, A. Kaldun, L. Argenti, P. Raith, K. Meyer, M. Laux, Y. Zhang, A. Blättermann, S. Hagstotz, T. Ding, R. Heck, J. Madroñero, F. Martín, and T. Pfeifer, *Nature* **516**, 374 (2014).
- [9] M. Kowalewski, K. Bennett, J. R. Rouxel, and S. Mukamel, *Phys. Rev. Lett.* **117**, 043201 (2016).
- [10] R. Kienberger, M. Hentschel, M. Uiberacker, C. Spielmann, M. Kitzler, A. Scrinzi, M. Wieland, T. Westerwalbesloh, U. Kleineberg, U. Heinzmann, M. Drescher, and F. Krausz, *Science* **297**, 1144 (2002).
- [11] U. Fröhling, M. Wieland, M. Gensch, T. Gebert, B. Schütte, M. Krikunova, R. Kalms, F. Budzyn, O. Grimm, J. Rossbach, E. Plönjes, and M. Drescher, *Nature Photonics* **3**, 523 (2009).
- [12] I. Grguraš, A. R. Maier, C. Behrens, T. Mazza, T. J. Kelly, P. Radcliffe, S. Düsterer, A. K. Kazansky, N. M. Kabachnik, T. Tschentscher, J. T. Costello, M. Meyer, M. C. Hoffmann, H. Schlarb, and A. L. Cavalieri, *Nature Photonics* **6**, 852 (2012).
- [13] W. Helml, A. R. Maier, W. Schweinberger, I. Grguraš, P. Radcliffe, G. Doumy, C. Roedig, J. Gagnon, M. Messerschmidt, S. Schorb, C. Bostedt, F. Grüner, L. F. DiMauro, D. Cubaynes, J. D. Bozek, T. Tschentscher, J. T. Costello, M. Meyer, R. Coffee, S. Düsterer, A. L. Cavalieri, and R. Kienberger, *Nature Photonics* **8**, 950 (2014).
- [14] Y. H. Jiang, A. Rudenko, J. F. Pérez-Torres, O. Herwerth, L. Foucar, M. Kurka, K. U. Kühnel, M. Toppin, E. Plésiat, F. Morales, F. Martín, M. Lezius, M. F. Kling, T. Jahnke, R. Dörner, J. L. Sanz-Vicario, J. van Tilborg, A. Belkacem, M. Schulz, K. Ueda, T. J. M. Zouros, S. Düsterer, R. Treusch, C. D. Schröter, R. Moshhammer, and J. Ullrich, *Phys. Rev. A* **81**, 051402 (2010).
- [15] S. Ackermann, A. Azima, S. Bajt, J. Bödewadt, F. Curbis, H. Dachraoui, H. Delsim-Hashemi, M. Drescher, S. Düsterer, B. Faatz, M. Felber, J. Feldhaus, E. Hass, U. Hipp, K. Honkavaara, R. Ischebeck, S. Khan, T. Laarmann, C. Lechner, T. Maltezopoulos, V. Miltchev, M. Mittenzwey, M. Rehders, J. Rönsch-Schulenburg, J. Rossbach, H. Schlarb, S. Schreiber, L. Schroedter, M. Schulz, S. Schulz, R. Tarkeshian, M. Tischer, V. Wacker, and M. Wieland, *Phys. Rev. Lett.* **111**, 114801 (2013).
- [16] J. Dalibard, Y. Castin, and K. Mølmer, *Phys. Rev. Lett.* **68**, 580 (1992).

SUPPLEMENTARY MATERIALS

Analysis of the streaking-Assisted Ionization

Assuming that the atom is subject to linearly polarized fields and the momentum distribution of photoelectrons, $w(p) = |p||M_p|^2$, is only collected along the polarization direction. The amplitude of the direct ionization with the strong field approximation (SFA) in the length gauge reads,

$$M_p(t) = \int_0^t dt' e^{iS_p(t')} \langle p + A(t') | \hat{\mu} E(t') | \Psi_0(t') \rangle \quad (5)$$

where $S_p(t) = \frac{1}{2} \int_0^t dt'' [p + A(t'')]^2$. The initial state may be prepared as the superposition of states $\{|\psi_i\rangle\}$ of the ionization energy $I_p^{(i)}$, $|\Psi_0(t')\rangle = \sum_i c_i(t') e^{iI_p^{(i)} t'} |\psi_i\rangle$. Substituting the superposition into Eq. (5),

$$M_p(t) = \sum_i \int_0^t dt' c_i(t') \mu_i[k(t')] E(t') e^{iS_{p,I_p^{(i)}}(t')}, \quad (6)$$

where $k(t') = p + A(t')$, the dipole matrix element $\mu_i(k) \equiv \langle k | \mu | \psi_i \rangle$ and the action $S_{p,I_p^{(i)}}(t) = \int_0^t dt'' \left[k(t'')^2/2 + I_p^{(i)} \right]$. Defining $M_p^{(i)}(t)$ the integral in Eq. (6), we recast $M_p(t) = \sum_i M_p^{(i)}(t)$ the superposition of transition amplitudes from all components of initial states.

Partial contribution from $M_p^{(i)}$

In the following we focus on the partial contribution $M_p^{(i)}$. If only the XUV pulse is present, $E(t') = E_{\text{XUV}}(t')$ and $A(t') = A_{\text{XUV}}(t')$. Since the amplitude $A_0^{(\text{XUV})} = E_0^{(\text{XUV})}/\omega_{\text{XUV}}$ is relatively small as ω_{XUV} is large, the action is reduced to $S_{p,I_p^{(i)}}^{(i)}(t') \simeq \int^t \left[\frac{1}{2} p^2 + I_p^{(i)} \right] dt'' = \left(\frac{1}{2} p^2 + I_p^{(i)} \right) t'$. Defining $E_{\text{XUV}}(t) = \mathcal{E}_{\text{XUV}}(t) \cos(\omega_{\text{XUV}} t)$ with \mathcal{E}_{XUV} the pulse envelope, the phase in the exponential reads $\frac{p^2}{2} + I_p^{(i)} \pm \omega_{\text{XUV}}$, and the fast oscillating part (the "+" term) can be neglected after the integration. Neglecting the dipole term, the transition amplitude is approximately

$$M_p^{(i)} \sim \int dt c_i(t) \mathcal{E}_{\text{XUV}}(t) e^{i\Omega_i(p)t}, \quad (7)$$

where $\Omega_i(p) = p^2/2 + I_p^{(i)} - \omega_{\text{XUV}}$. It can be viewed as the short time Fourier transform of $c_i(t)$ with the window function $\mathcal{E}_{\text{XUV}}(t)$. The spectrum $|M_p^{(i)}|^2$ peaks at $p^2/2 = \omega_{\text{XUV}} - I_p^{(i)}$.

With the presence of both XUV and THz pulses, since $A_0^{(\text{XUV})} \ll A_0^{(\text{THz})}$ and $E_0^{(\text{XUV})} > E_0^{(\text{THz})}$, $k(t') \simeq$

$p + A_{\text{THz}}(t')$. Since the XUV pulse is around the center of the THz field and the duration of the former is much smaller than the latter, the THz field is approximately linear, $A_{\text{THz}}(t) \simeq \alpha(t - \tau)$, around the streaking time when ionization events occur. Conducting the series expansion around the center of $A_{\text{THz}}(t)$, it is shown that the slope $\alpha = -E_0^{(\text{THz})}$. Substituting the linear approximation of $A_{\text{THz}}(t)$ into action $S_{p, I_p}^{(i)}(t')$, we find $S_{p, I_p}^{(i)}(t) = \frac{\alpha^2}{6}t^3 + \left(\frac{\alpha p}{2} - \frac{\alpha^2}{2}\tau\right)t^2 + \left(\frac{p^2}{2} + I_p^{(i)} - \alpha p\tau + \frac{\alpha^2\tau^2}{2}\right)t$. The

cubic term is negligible when α is small, thus $S_{p, I_p}^{(i)}(t) \simeq \frac{\alpha p}{2}t^2 + \left(\frac{p^2}{2} + I_p^{(i)} - \alpha p\tau\right)t = \frac{\alpha p}{2}(t - \tau)^2 + \left(\frac{p^2}{2} + I_p^{(i)}\right)(t - \tau) + \phi_i(p, \tau)$ with $\phi_i(p, \tau) = \left(\frac{p^2}{2} + I_p^{(i)}\right)\tau - (\alpha p/2)\tau^2$ a phase that can be factored out of the integration over t . Similar to the analysis without the THz streaking, the transition amplitude in the polarization direction is given by

$$M_p^{(i)} \sim \frac{1}{2} e^{i\phi_i(p, \tau)} \int dt c_i(t) \mathcal{E}_{\text{XUV}}(t - \tau) e^{i\left[\frac{\alpha p}{2}(t - \tau)^2 + \Omega_i(p)(t - \tau)\right]}, \quad (8)$$

as long as the occurrence of XUV field is within the linear region of the THz field. Comparing with Eq. (7), the appearance of an extra quadratic term in the exponent, $(\alpha p/2)(t - \tau)^2$, results in the spectral broadening, as is shown in the next paragraph.

Broadening of spectral peaks by THz-streaking field

Assuming that the amplitude of wave function, $c_i(t)$, varies slowly and the amplitude roughly remains a constant, $c_i(t) \equiv c_i$. When the envelope of the XUV pulse is Gaussian, $\mathcal{E}_{\text{XUV}}(t - \tau) = E_0^{(\text{XUV})} e^{-(t - \tau)^2/\sigma^2}$, the tran-

sition amplitude from Eq. (8) reads

$$M_p^{(i)} \sim \frac{1}{2} c_i e^{i\phi_i(p, \tau)} E_0^{(\text{XUV})} \sqrt{\frac{\pi}{b(p)}} e^{-\frac{\Omega_i^2(p)}{4b(p)}} \quad (9)$$

with parameter $b(p) = 1/\sigma^2 - i(\alpha p/2)$ determining the width of the spectral peak. The extra term $-i(\alpha p/2)$ accounts for the broadening induced by the THz streaking. Turning the THz field on, the spectral width increases from $2/\sigma^2$ to $2/\sigma^2 + (\alpha p\sigma)^2/2$.

Ionization probability and momentum distribution

In the following we calculate the ionization signal based on the partial contribution of Eq. (8). When the wave function varies slowly, the ionization signal is evaluated by

$$\begin{aligned} |M_p|^2 &\sim \left| \sum_i \frac{1}{2} c_i e^{i\phi_i(p, \tau)} E_0^{(\text{XUV})} \sqrt{\frac{\pi}{b(p)}} e^{-\frac{\Omega_i^2(p)}{4b(p)}} \right|^2 \\ &= \frac{\pi (E_0^{(\text{XUV})})^2}{|b(p)|} \left\{ \sum_i |c_i|^2 e^{-\frac{\Omega_i^2(p)}{2|b(p)|\sigma^2}} + \sum_{i, j \neq i} (c_i^* c_j) e^{i(\phi_j(p, \tau) - \phi_i(p, \tau))} e^{-\left[\frac{\Omega_i^2(p)}{4b^*(p)} + \frac{\Omega_j^2(p)}{4b(p)}\right]} \right\}. \quad (10) \end{aligned}$$

Firstly, the difference of phase factor recovers the coherence term, $\phi_j(p, \tau) - \phi_i(p, \tau) = (I_p^{(j)} - I_p^{(i)})\tau$. It indicates that scanning over the time delay τ results in an

oscillating patterns that maps the coherence beating. In addition, the exponent in the last term that describes the contribution from the coherence can be reduced to

$$\begin{aligned}
-\left[\frac{\Omega_i^2}{4b^*} + \frac{\Omega_j^2}{4b}\right] &= \frac{1}{4[(1/\sigma^2)^2 + (\alpha p/2)^2]} \left[-\frac{\Omega_i^2 + \Omega_j^2}{\sigma^2} + i\left(\frac{\alpha p}{2}\right)(\Omega_i^2 - \Omega_j^2) \right] \\
&= \frac{1}{2[(1/\sigma^2)^2 + (\alpha p/2)^2]} \left[-\frac{\Omega_{ij}^2 + (\Delta_{ij}/2)^2}{\sigma^2} + i\left(\frac{\alpha p}{2}\right)\Delta_{ij}\Omega_{ij} \right] \\
&= -\frac{\Omega_{ij}^2}{2|b(p)|^2\sigma^2} - \frac{(\Delta_{ij}/2)^2}{2|b(p)|^2\sigma^2} + i\frac{\alpha p\Delta_{ij}\Omega_{ij}}{4|b(p)|^2},
\end{aligned}$$

where $\Omega_{ij}(p) = \frac{p^2}{2} + \frac{I_p^{(i)} + I_p^{(j)}}{2} - \omega$ and $\Delta_{ij} = I_p^{(i)} - I_p^{(j)}$.

In the final form, we have

$$|M_p|^2 \sim \frac{\pi(E_0^{(XUV)})^2}{|b(p)|} \left\{ \sum_i |c_i|^2 e^{-\frac{\Omega_i^2(p)}{2|b(p)\sigma|^2}} + \sum_{i,j \neq i} (c_i^* c_j) e^{-i\Delta_{ij}\tau} e^{-\frac{\Omega_{ij}^2(p)}{2|b(p)\sigma|^2}} e^{-\frac{(\Delta_{ij}/2)^2}{2|b(p)\sigma|^2}} e^{-i\frac{\alpha p\Delta_{ij}\Omega_{ij}(p)}{4|b(p)|^2}} \right\}. \quad (11)$$

From Eq. (11) possesses several main features of the photoelectronic spectrum in the streaking regime,

- From the Gaussian factor, the population peak of state i appears at $\Omega_i(p) = 0$, $p^2/2 = \omega - I_p^{(i)}$, while the coherence peak of states i and j appears at $\Omega_{ij}(p) = 0$, $p^2/2 = \omega - (I_p^{(i)} + I_p^{(j)})/2$, which is exactly located at the center of two relevant population peaks.
- The coherence term is typically much smaller than the population term due to the second factor $e^{-(\Delta_{ij}/2)^2/(2|b(p)\sigma|^2)}$.
- With the THz streaking, the denominator $|b(p)\sigma|^2$ increases and the signal of the coherence term is relatively enhanced.
- The last term suggests the momentum distribution may also oscillates with p . The difference between the forward and backward momentum distribution can be referred from the last term when we change $p \rightarrow -p$.
- We should mention the above formula have neglected the contributions from the dipole matrix elements and the latter contains structural information of the atom.

Method of Monte Carlo wave function (MCWF)

The implementation of the MCWF, which also includes the dissipation process, may be referred to [16]. The

Rabi frequency $\Omega = 0.02$, the optical frequency $\omega_c = 0.375$. The envelope of the light field is given by $E(t) = e^{-(t-t_c)^2/\sigma^2}$ with $t_c = 4150$ and $\sigma = 60$.

The quantum evolution for the two-level system $|\Psi\rangle = c_0|0\rangle + c_1|1\rangle$ is governed by the EOM

$$\begin{pmatrix} \dot{c}_0 \\ \dot{c}_1 \end{pmatrix} = -i \begin{pmatrix} \omega_0 & E(t)\Omega \cos(\omega_c t) \\ E(t)\Omega \cos(\omega_c t) & \omega_1 \end{pmatrix} \begin{pmatrix} c_0 \\ c_1 \end{pmatrix}.$$

In the interaction picture by substituting $c_i = \tilde{c}_i e^{-i\omega_i t}$ and using the RWA, the EOM reads

$$\begin{pmatrix} \dot{\tilde{c}}_0 \\ \dot{\tilde{c}}_1 \end{pmatrix} = -i\frac{\Omega}{2}E(t) \begin{pmatrix} 0 & e^{-i\delta t} \\ e^{+i\delta t} & 0 \end{pmatrix} \begin{pmatrix} \tilde{c}_0 \\ \tilde{c}_1 \end{pmatrix},$$

where the detuning is defined by $\delta = \omega_a - \omega_c$. Here for $\omega_0 = -0.5$ and $\omega_1 = -0.125$, the resonance condition is satisfied, $\delta = 0$. The initial state is in the $|0\rangle$ state.

The MCWF allows the quantum jump from state $|1\rangle$ to $|0\rangle$ during the evolution of the wave function. Defining the jump rate Γ , the quantum jump occurs when $\Gamma|c_1|^2 dt > \varepsilon$, where ε is a uniformly distributed random number in the range $[0, 1)$. Here we set $\Gamma = 0.008$. An ensemble consisting of 100 different wave functions is generated and the amplitudes $c_i(t)$ are stored for the calculation of momentum distribution.